

Microscopic analysis of the giant monopole resonance excitation energy

M. K. Gaidarov,^{1,2} M. V. Ivanov,^{1,2} Y. I. Katsarov,¹ A. N. Antonov,¹ and I. C. Danchev³

¹*Institute for Nuclear Research and Nuclear Energy,
Bulgarian Academy of Sciences, Sofia 1784, Bulgaria*

²*Department of Physics, Faculty of Mathematics and Natural Sciences,
South-West University "Neofit Rilski", Blagoevgrad, Bulgaria*

³*Department of Physical and Mathematical Sciences,
School of Arts and Sciences, University of Mount Olive,
652 R.B. Butler Dr., Mount Olive, NC 28365, USA*

A systematic study of the isoscalar giant monopole resonance (ISGMR) in a wide range of nuclei from various isotopic chains is performed within the microscopic self-consistent Skyrme HF+BCS method and coherent density fluctuation model (CDFM). The calculations for the nuclear incompressibility are based on the Brueckner and Barcelona-Catania-Paris-Madrid (BCPM) energy density functionals for nuclear matter using the capability of the CDFM to make a transition to the corresponding incompressibility in finite nuclei. The results obtained by applying of different definitions of the ISGMR energy, as well as the two energy-density functionals, are analyzed and compared with the available experimental data. The consideration includes the peculiarities of the proton and neutron density distributions and their corresponding linear size characteristics. In general, a connection with the measured neutron skin thicknesses is proposed as a possible way for realistic estimations of the energy of ISGMR.

PACS numbers: 24.30.Cz, 21.10.Gv, 21.60.-n, 21.65.+f

I. INTRODUCTION

The great interest to study the giant resonances both experimentally and theoretically is provoked by the fundamental understanding of the nonequilibrium properties of nuclei and the nuclear force. Particularly, the isoscalar giant monopole resonance (ISGMR) measures the collective response of the nucleus to density fluctuations. The energy of this resonance is connected to the incompressibility of the nucleus, which, in turn, can be linked to the incompressibility of the infinite nuclear matter, which is an important ingredient of the nuclear matter equation of state (EOS). The EOS plays significant role in the description of heavy-ion nuclear collision [1], the collapse of the heavy stars in super novae explosions [2, 3] and some astrophysical quantities, such as radii and masses of neutron stars [4]. The 20% uncertainty of the currently accepted value of the incompressibility of nuclear matter is largely driven by the poor determination of the EOS isospin asymmetry term [5]. To improve upon the precision of this term, experimental measurements of isoscalar monopole modes are being carried out on isotopic chains, with an extension from the nuclei on the valley of stability towards exotic nuclei with large proton-neutron asymmetry. On the other side, theoretical estimations of the giant monopole excitation energies have been made for nuclei in the super heavy region for $Z = 114$ and 120, which are predicted by several models as the next proton magic numbers beyond $Z = 82$ [6].

An important primary motivation for studying the ISGMR is to probe bulk nuclear properties of the nuclear EOS. As such, it is highly unexpected that effects arising from microscopic shell structure would appreciably influence the collective behavior of the nucleus under-

going these excitations. The isoscalar resonances are excited through low-momentum transfer reactions in inverse kinematics, that require special detection devices. At present, promising results have been obtained using active targets. Different measurements have been conducted on Ni isotopes far from stability, namely ^{56}Ni [7, 8] and ^{68}Ni [9, 10]. In particular, the experiment with ^{68}Ni is the first measurement of the isoscalar monopole response in a short-lived neutron-rich nucleus using inelastic alpha scattering. The ISGMR was found to be fragmented, with a possible indication for the soft monopole resonance. Complementary to using inelastic scattering of α -particles, which has been used to great effect over the last several decades, in Ref. [11] the use of ^6Li as a probe to study the ISGMR in several stable nuclei (^{58}Ni , ^{90}Zr , ^{116}Sn , and ^{208}Pb) was explored. The measured inelastic scattering spectra have shown to agree very well with the previously measured ISGMR responses from α -particle scattering, thus manifesting the feasibility of employing ^6Li inelastic scattering in investigations of the ISGMR.

The discussion on how to extract the incompressibility of nuclear matter from the ISGMR dates back to the years 1980s [12, 13] (see also more recent review [14]). The measurement of the centroid energy of the ISGMR [15–21] provides a very sensitive method to determine the incompressibility value. Theoretical investigations in various models [22–28] with grouped values of the nuclear matter incompressibility predict different ISGMR energies. The comparison with the experimental excitation energies of the ISGMR in finite nuclei could give the constraint on the nuclear matter incompressibility modulus.

In the present work the incompressibility and the centroid energy of ISGMR are studied *in a wide range of*

finite nuclei on the basis of the Brueckner [29, 30] as well as BCPM [31–33] functionals for nuclear matter and using the coherent density fluctuation model (CDFM) (e.g., Refs. [34, 35]). The latter is a natural extension of the Fermi gas model based on the generator coordinate method [35, 36] and includes long-range correlations of collective type. In our previous works [34, 35, 37–44] we have demonstrated the capability of CDFM to be applied as an alternative way to make a transition from the properties of nuclear matter to those of finite nuclei investigating the ISGMR, the nuclear symmetry energy (NSE), the neutron pressure, and the asymmetric compressibility in finite nuclei. While there is enough collected information for these key EOS parameters (although the uncertainty of their determination is still large), the volume and surface symmetry energies have been poorly investigated till now. Therefore, in Ref. [45] we proposed a new alternative approach to calculate the ratio of the surface to volume components of the NSE in the framework of the CDFM. We have demonstrated that the new scheme leads to more realistic values that agree better with the empirical data and exhibits conceptual and operational advantages.

A first attempt to study the ISGMR in Ni, Sn, and Pb isotopes within the microscopic self-consistent Skyrme HF+BCS method and CDFM was performed in our previous work [46]. The calculations were based on the Brueckner energy-density functional (EDF) for nuclear matter. The obtained results have demonstrated the relevance of the proposed theoretical approach to probe the excitation energy of the ISGMR in various nuclei. On the other hand, however, it became clear that another, more refined method for calculations of the nuclear compressibility has to be used, as well as more realistic EDFs to be employed in the calculations of the monopole excitation energy for wider spectrum of nuclei.

In the present work, we perform calculations using an extended method to calculate the incompressibility and ISGMR energy in nuclei, in which EDFs of Brueckner *et al.* [29, 30] and BCPM [31–33] are adopted. The results for the excitation energies of ISGMR are obtained by using its two definitions given in literature. Apart from these complimentary considerations, in this work a variety of different even-even nuclei from ^{40}Ca to ^{208}Pb is considered and results for the energy of the ISGMR are presented and discussed in comparison with the experimental data. In addition, we analyze the values of the centroid energies of Sn isotopes ($A = 112 - 124$), as well as ^{48}Ca and ^{208}Pb nuclei, studying their isotopic sensitivity by adding results on the base of experimentally measured neutron skin thickness.

The structure of this paper is the following. In Section II we present the theoretical scheme that includes the common definitions of the excitation energy of ISGMR and properties of nuclear matter characterizing its density dependence around normal nuclear matter density, as well as the CDFM formalism, which provides a way to calculate starting from nuclear matter quantities

the corresponding ones in finite nuclei. Some of the relationships are given in Appendix A. Section III contains the numerical results and discussion. The summary and main conclusions of the study are given in Section IV.

II. THEORETICAL SCHEME

A. Excitation energy of the ISGMR

In this subsection we present the relationships used to obtain the energy of the ISGMR through the incompressibility K^A of a nucleus with Z protons and N neutrons. Basically there are two definitions which will be used further in our calculations. One of them is (see Ref. [22])

$$E_{\text{ISGMR}} = \frac{\hbar}{r_0 A^{1/3}} \sqrt{\frac{K^A}{m}}, \quad (1)$$

where $A = Z + N$ is the mass number, m is the nucleon mass and r_0 is a radius parameter deduced from the equilibrium density.

The second definition is given in the scaling method [47] (see, e.g., Refs. [16, 17]) as

$$E_{\text{ISGMR}} = \hbar \sqrt{\frac{K^A}{m < r^2 >}}, \quad (2)$$

where $< r^2 >$ is the mean square mass radius of the nucleus in the ground state.

We note that Eq. (2) does not contain a fit parameter and directly uses the radii obtained from mean-field calculations. The results obtained by the usage of Eqs. (1) and (2) will be shown and discussed in Section III. Also, the variations related with parameter r_0 for different nuclei and the comparison with some results obtained by using $< r^2 >$ will be presented there.

B. The relation between the key EOS parameters in nuclear matter and finite nuclei in the CDFM

First, we will give briefly the main relationships of the CDFM which was suggested and developed in Refs. [34, 35]. For the purposes of the present work we should mention our recent papers [38, 42, 45] in which CDFM was intensively used. In it the one-body density matrix (OBDM) $\rho(\mathbf{r}, \mathbf{r}')$ of the nucleus is a superposition of OBDM's $\rho_x(\mathbf{r}, \mathbf{r}')$ of spherical “pieces” of nuclear matter (called “fluctons”) with radius x in which all A nucleons are uniformly distributed:

$$\rho(\mathbf{r}, \mathbf{r}') = \int_0^\infty dx |F(x)|^2 \rho_x(\mathbf{r}, \mathbf{r}') \quad (3)$$

with

$$\begin{aligned} \rho_x(\mathbf{r}, \mathbf{r}') &= 3\rho_0(x) \frac{j_1(k_F(x)|\mathbf{r} - \mathbf{r}'|)}{(k_F(x)|\mathbf{r} - \mathbf{r}'|)} \\ &\times \Theta\left(x - \frac{|\mathbf{r} + \mathbf{r}'|}{2}\right), \end{aligned} \quad (4)$$

where

$$\Theta(y) = \begin{cases} 1, & y \geq 0 \\ 0, & y < 0 \end{cases} \quad (5)$$

is the step-function of Heaviside. In Eq. (4)

$$\rho_0(x) = \frac{3A}{4\pi x^3}, \quad (6)$$

$$k_F(x) = \left(\frac{3\pi^2}{2} \rho_0(x) \right)^{1/3} \equiv \frac{\alpha}{x} \quad (7)$$

with

$$\alpha = \left(\frac{9\pi A}{8} \right)^{1/3} \simeq 1.52A^{1/3} \quad (8)$$

and j_1 is the first-order spherical Bessel function.

The nucleon density distribution is given by the diagonal elements of the OBDM (3):

$$\rho(\mathbf{r}) = \rho(\mathbf{r}, \mathbf{r}) = \int_0^\infty dx |F(x)|^2 \rho_0(x) \Theta(x - |\mathbf{r}|). \quad (9)$$

It can be seen from Eq. (9) that in the case of monotonically decreasing local density ($d\rho/dr \leq 0$) the weight function $|F(x)|^2$ in CDFM can be obtained:

$$|F(x)|^2 = -\frac{1}{\rho_0(x)} \left. \frac{d\rho(r)}{dr} \right|_{r=x}. \quad (10)$$

It is normalized as

$$\int_0^\infty dx |F(x)|^2 = 1. \quad (11)$$

Second, we give the main relationships for the symmetry energy of nuclear matter (NM) $S(\rho)$, that is related to the energy density $\varepsilon(\rho_p(\mathbf{r}), \rho_n(\mathbf{r}))$, the latter depending on proton and neutron densities, and the asymmetry

$$\delta = \frac{\rho_n - \rho_p}{\rho_n + \rho_p}.$$

The expansion of ε in δ up to the quadratic term in asymmetric NM has the form:

$$\varepsilon(\rho, \delta) = \varepsilon_0(\rho, \delta = 0) + \rho S(\rho) \delta^2, \quad (12)$$

where $\varepsilon_0(\rho, \delta = 0)$ is the energy density of symmetric NM. The second term contains the symmetry energy of NM:

$$S(\rho) = \frac{1}{2} \left. \frac{\partial^2 \left(\frac{\varepsilon(\rho, \delta)}{\rho} \right)}{\partial \delta^2} \right|_{\delta=0} \quad (13)$$

(see, e.g. [45, 48–50]). Here we remind the relation of $\varepsilon(\rho, \delta)$ to the energy per particle E/A :

$$\frac{\varepsilon(\rho, \delta)}{\rho} = \frac{E(\rho, \delta)}{A}.$$

In the CDFM scheme, the symmetry energy of *finite nuclei* has the form:

$$S^A = \int_0^\infty dx |F(x)|^2 S(\rho_0(x)), \quad (14)$$

where the weight function $|F(x)|^2$ is given by Eqs. (10) and (11).

Next, we consider the incompressibility in *finite nuclei* K^A , which in the CDFM is written in the form

$$K^A = \int_0^\infty dx |F(x)|^2 K(\rho_0(x)). \quad (15)$$

In Eq. (15) the weight function $|F(x)|^2$ is obtained using Eqs. (10) and (11), similarly as in Eq. (14).

The function $K(\rho_0(x))$ in the integrand of Eq. (15) is the incompressibility in infinite nuclear matter. The latter has the form (see, e.g. [50]):

$$K(\rho_0(x)) = K_{NM}(\rho_0(x)) + K_\tau(\rho_0(x)) \delta^2 + K_{Coul}(\rho_0(x)) \frac{Z^2}{A^{4/3}}. \quad (16)$$

The components of $K(\rho_0(x))$ in Eq. (16) are as follows:

(i)

$$K_{NM}(\rho_0(x)) = 9\rho_0^2(x) \left. \frac{\partial^2 \left(\frac{\varepsilon(\rho, \delta=0)}{\rho} \right)}{\partial \rho^2} \right|_{\rho=\rho_0(x)} \quad (17)$$

is the incompressibility of *symmetric* NM (known also as K_∞ or “the volume term” K_{vol} , see Ref. [50]);

(ii) The asymmetry term of the NM incompressibility:

$$K_\tau(\rho_0(x)) = K_{sym}(\rho_0(x)) - \frac{L_{sym}(\rho_0(x)) Q(\rho_0(x))}{K_{NM}(\rho_0(x))} \quad (18)$$

or

$$K_\tau(\rho_0(x)) = K_{sym}(\rho_0(x)) + 3L_{sym}(\rho_0(x)) - L_{sym}(\rho_0(x)) B(\rho_0(x)), \quad (19)$$

where

$$K_{sym}(\rho_0(x)) = 9\rho_0^2(x) \left. \frac{\partial^2 S(\rho)}{\partial \rho^2} \right|_{\rho=\rho_0(x)}. \quad (20)$$

The function L_{sym} in Eqs. (18) and (19) is known as a “slope parameter” and has the form:

$$L_{sym}(\rho_0(x)) = 3\rho_0(x) \left. \frac{\partial S(\rho)}{\partial \rho} \right|_{\rho=\rho_0(x)}. \quad (21)$$

The functions $Q(\rho_0(x))$ and $B(\rho_0(x))$ in Eqs. (18) and (19) are defined as follows:

$$Q(\rho_0(x)) = 27\rho_0^3(x) \left. \frac{\partial^3 \left(\frac{\varepsilon(\rho, \delta=0)}{\rho} \right)}{\partial \rho^3} \right|_{\rho=\rho_0(x)} \quad (22)$$

and

$$B(\rho_0(x)) = \frac{27\rho_0^2}{K_{NM}(\rho_0(x))} \left. \frac{\partial^3 \varepsilon(\rho, \delta=0)}{\partial \rho^3} \right|_{\rho=\rho_0(x)}. \quad (23)$$

The latter function can be written also as:

$$B(\rho_0(x)) = 9 + \frac{Q(\rho_0(x))}{K_{NM}(\rho_0(x))}. \quad (24)$$

In our previous work [46] we have used the notation ΔK^{NM} instead of K_{sym} from Eq. (20).

(iii) The Coulomb term is given by:

$$K_{Coul}(\rho_0(x)) = \frac{3}{5} \frac{e^2}{r_0(x)} (1 - B(\rho_0(x))) \quad (25)$$

with $e^2 \cong 1.44$ MeV.fm and

$$r_0(x) = \left(\frac{3}{4\pi \rho_0(x)} \right)^{1/3}. \quad (26)$$

Here we should mention the formal partial similarity of Eq. (16) with Eq. (18) in Ref. [50]. The latter gives the incompressibility for finite nuclei, while our Eq. (16) is for the incompressibility in nuclear matter. Eq. (18) in Ref. [50] accounts for the surface contribution, while in our case Eq. (15) makes a transition from $K(\rho_0(x))$ in NM to K^A in *finite nuclei*, accounting for the surface contributions weighting $K(\rho_0(x))$ by the weight function $|F(x)|^2$, which is related to the density distribution of a given nucleus.

C. Brueckner and Barcelona-Catania-Paris-Madrid EDFs

In what follows we give the expressions for the EDFs used in the present work. We consider the energy as a sum of the kinetic $T(\rho, \alpha)$ and the potential $V(\rho, \alpha)$ contributions

$$\frac{E(\rho, \alpha)}{A} = T(\rho, \alpha) + V(\rho, \alpha), \quad \alpha = \frac{N - Z}{A} \quad (27)$$

in both approaches for EDF's, namely that one of Brueckner [29, 30, 51] and of the Barcelona-Catania-Paris-Madrid (BCPM) one (see, e.g. Ref. [31–33] and references therein).

The kinetic energy part of the EDF used is of the Thomas-Fermi type:

$$T(\rho, \alpha) = \frac{C}{2} [(1 + \alpha)^{5/3} + (1 - \alpha)^{5/3}] \rho^{2/3}. \quad (28)$$

We use two types of the potential part of the EDF $V(\rho, \alpha)$:

i) That one from the Brueckner EDF [30, 51]:

$$V(\rho, \alpha) = b_1 \rho + b_2 \rho^{4/3} + b_3 \rho^{5/3} + \alpha^2 (b_4 \rho + b_5 \rho^{4/3} + b_6 \rho^{5/3}) \quad (29)$$

and

ii) The potential part of the BCPM EDF (see, e.g. Ref. [31]):

$$V(\rho, \alpha) = \sum_{n=1}^5 a_n \left(\frac{\rho}{\rho_\infty} \right)^n (1 - \alpha^2) + \sum_{n=1}^5 b_n \left(\frac{\rho}{\rho_{0n}} \right)^n \alpha^2. \quad (30)$$

The values of the parameters a_n and b_n in Eq. (30), as well as $\rho_\infty = 0.16$ fm⁻³ and $\rho_{0n} = 0.155$ fm⁻³ are given in Ref. [31].

In Eqs. (28) and (29) the values of the parameters C and $b_1 \div b_6$ are listed in Appendix A [see Eqs. (A6) and (A7)]. The expressions for the quantities $S(\rho_0(x))$ [Eq. (13)], $K_{NM}(\rho_0(x))$ [Eq. (17)], $K_{sym}(\rho_0(x))$ [Eq. (20)], $L_{sym}(\rho_0(x))$ [Eq. (21)], $Q(\rho_0(x))$ [Eq. (22)] and $B(\rho_0(x))$ [Eqs. (23) and (24)] obtained in our work for the cases of the Brueckner [29, 30, 51] and BCPM EDF (see, e.g. Ref. [31] and references therein), are given in Appendix A.

III. RESULTS AND DISCUSSION

In the calculations the density distributions $\rho(r)$, which are necessary to compute the weight function $|F(x)|^2$ [Eq. (10)], are obtained within the self-consistent deformed Hartree-Fock method with density-dependent SLy4 interaction [52] and pairing correlations [53] (see also Refs. [37–40, 42, 54]). The expressions for the single-particle wave functions and densities $\rho_{p,n}(r)$ in the mentioned method are given, e.g., in Ref. [37].

The mean square radii for protons and neutrons are obtained using the corresponding definitions:

$$\langle r_{p,n}^2 \rangle = \frac{\int r^2 \rho_{p,n}(\mathbf{r}) d\mathbf{r}}{\int \rho_{p,n}(\mathbf{r}) d\mathbf{r}}, \quad (31)$$

while the matter mean square radius $\langle r^2 \rangle$ entering Eq. (2) can be calculated by the expression:

$$\langle r^2 \rangle = \frac{N}{A} \langle r_n^2 \rangle + \frac{Z}{A} \langle r_p^2 \rangle. \quad (32)$$

We start our analysis by calculating the NSE and some parameters related to its density dependence. The values of the symmetry energy S^A , the slope parameter L_{sym}^A , and skewness parameter Q^A in a wide range of nuclei from ⁴⁰Ca to ²⁰⁸Pb obtained using EDF's of Brueckner and $V(\rho, \alpha)$ from BCPM [further called BCPM(v)] are given in Table I. Similarly to Eqs. (14) and (15), the skewness parameter Q^A for finite nuclei can be calculated

in the CDFM scheme. The values of the symmetry energies S^A deduced from the calculations with both EDF's are realistic lying in the interval between 25 and 30 MeV. Concerning the values of the slope parameter, it can be seen from Table I that the BCPM(v) functional produces almost twice larger values compared with the L_{sym}^A values obtained using the Brueckner EDF. For instance, the calculations based on interactions derived from chiral effective field theory (EFT) predict for ^{208}Pb nucleus values for the symmetry energy of 31.3 ± 0.8 MeV and slope parameter of 52.6 ± 4.0 MeV [55]. The use of the BCPM(v) functional leads to values for these two characteristics of ^{208}Pb , which are very close to the ones obtained in Ref. [55] (see Table I). Therefore, this is a good starting point to study further quantities such as the intrinsic symmetry energy parameter, namely the incompressibility K^A , and the mean square nuclear radius $\langle r^2 \rangle$ that are basic ingredients to calculate the monopole excitation energy.

In Table II are shown the values of the incompressibility K^A and its components K_{NM}^A , K_τ^A and K_{Coul}^A in the same range of nuclei calculated using EDF of Brueckner and BCPM(v). While the differences of the symmetry energy S^A for both EDFs which can be seen in Table I are relatively small (2.26 MeV, 2.49 MeV, 1.88 MeV for ^{40}Ca , ^{56}Ni , and ^{106}Cd , respectively) there are large differences in the value of K^A .

The corresponding energy E_{ISGMR} calculated in the present work using Eq. (2) are also given in Table II and are compared with the available experimental data for the same range of nuclei. We should mention that the results for the centroid energy in the case of the Brueckner EDF are in good agreement with the data for isotopes of Ca, Fe, and Ni and acceptable for those of Zn, Mo, and Cd. In the case of BCPM(v) EDF they are comparable in the case of ^{68}Ni and partly for some isotopes of Pb. The use of Eq. (2) includes the calculations of two quantities, namely, the incompressibility $K^A(N, Z)$ which is obtained by Eqs. (15)-(20) and (25)-(26), and the rms radii $\langle r^2 \rangle^{1/2}$ which are calculated by Eqs. (31) and (32) using density distributions obtained within the self-consistent deformed Hartree-Fock method with SLy4 effective Skyrme force and with pairing correlations.

Concerning the use of Eq. (2), in particular the nuclear rms radii in it, we would like to note the following: i) the rms radii can be calculated on the base of experimentally obtained proton density distributions by means of electromagnetic interaction and some other processes; ii) while in many cases the charge densities are well known (see, e.g., Ref. [61]) with relatively high accuracy, this is not the case with the neutron densities which could not be precisely obtained due to the charge neutrality of the neutrons. Thus, there is generally a lack of data for the neutron density, or their knowledge comes only from a small number of specific experiments. In the majority of cases the neutron density is used on the base of some approximations of the proton densities. In many cases (as in the present work) estimations of the proton and neu-

TABLE I: The values of the symmetry energy S^A [Eq. (14)], slope parameter L_{sym}^A [Eq. (21)], and skewness parameter Q^A of the considered nuclei calculated within the CDFM by using Brueckner and BCPM(v) energy-density functionals.

Nuclei	Brueckner			BCPM(v)		
	S^A [MeV]	L_{sym}^A [MeV]	Q^A [MeV]	S^A [MeV]	L_{sym}^A [MeV]	Q^A [MeV]
^{40}Ca	25.61	25.16	-373.66	27.87	53.19	-257.59
^{42}Ca	25.86	25.13	-379.65	28.17	53.65	-264.48
^{44}Ca	26.11	25.01	-385.80	28.45	54.10	-271.41
^{46}Ca	26.35	25.22	-390.29	28.66	54.36	-289.03
^{48}Ca	26.66	24.92	-399.06	29.03	54.97	-298.20
^{54}Fe	27.34	24.82	-415.00	29.78	56.13	-322.20
^{56}Ni	27.58	24.64	-421.61	30.06	56.58	-330.95
^{58}Ni	27.24	24.29	-416.26	29.73	56.08	-315.65
^{60}Ni	26.98	24.02	-412.14	29.47	55.67	-305.05
^{68}Ni	27.00	25.67	-403.01	29.28	55.07	-326.62
^{64}Zn	26.65	24.57	-401.57	29.03	54.85	-300.56
^{68}Zn	26.75	25.40	-399.03	29.05	54.75	-311.96
^{90}Zr	27.94	28.56	-408.56	29.85	55.21	-419.70
^{92}Zr	27.68	27.94	-406.37	29.67	55.07	-397.63
^{92}Mo	28.02	28.54	-410.60	29.95	55.36	-422.09
^{94}Mo	27.79	28.20	-407.30	29.74	55.10	-407.35
^{96}Mo	27.59	27.93	-404.35	29.55	54.85	-395.98
^{106}Cd	27.93	28.73	-407.78	29.81	55.06	-423.52
^{110}Cd	27.90	29.12	-404.73	29.72	54.86	-426.21
^{112}Cd	27.89	29.18	-404.20	29.72	54.84	-425.20
^{114}Cd	27.89	29.41	-402.87	29.68	54.73	-429.10
^{116}Cd	27.88	29.58	-401.85	29.64	54.64	-432.47
^{100}Sn	28.59	29.28	-419.35	30.44	55.94	-461.83
^{112}Sn	28.12	29.25	-409.10	29.95	55.17	-438.16
^{114}Sn	28.12	29.51	-407.63	29.91	55.05	-442.58
^{116}Sn	28.12	29.70	-406.48	29.87	54.95	-446.28
^{118}Sn	28.12	29.65	-406.71	29.88	54.98	-444.29
^{120}Sn	28.12	29.78	-406.20	29.87	54.92	-447.63
^{122}Sn	28.15	29.75	-407.02	29.91	54.98	-447.61
^{124}Sn	28.21	29.96	-407.10	29.93	54.96	-454.81
^{132}Sn	28.63	30.70	-412.58	30.26	55.26	-490.43
^{204}Pb	28.93	33.65	-403.13	30.17	54.38	-544.21
^{206}Pb	28.93	33.44	-404.28	30.20	54.45	-541.14
^{208}Pb	28.91	33.27	-404.90	30.20	54.47	-539.23

tron densities obtained in various theoretical methods are used.

The above mentioned points (i) and (ii) are particularly related to the neutron-rich nuclei, which are the majority of the considered nuclei. Among the latter there are four neutron-rich exotic nuclei with short half-life time, namely ^{56}Ni , ^{68}Ni , ^{100}Sn , and ^{132}Sn . The reasons mentioned above lead to certain difficulties, namely reliable total nucleon density distributions ($\rho = \rho_p + \rho_n$) to be used in the calculations of the rms radii which enter Eq. (2).

Along this line our next step is to consider the rare cases, where data extracted for the neutron skin thickness with probes having different sensitivities to the proton and neutron distributions are available. As an example,

TABLE II: The values of nuclear properties, including K_{NM}^A , K_τ^A , K_{Coul}^A , K^A , and E_{ISGMR} calculated using Brueckner and BCPM(v) EDFs and Eq. (2), along with rms radii and experimental data for the ISGMR energy.

Nuclei	Brueckner					BCPM(v)					$\langle r^2 \rangle^{1/2}$ [fm]	Exp. [MeV]
	K_{NM}^A [MeV]	K_τ^A [MeV]	K_{Coul}^A [MeV]	K^A [MeV]	E_{ISGMR} [MeV]	K_{NM}^A [MeV]	K_τ^A [MeV]	K_{Coul}^A [MeV]	K^A [MeV]	E_{ISGMR} [MeV]		
^{40}Ca	118.78	-367.82	-3.50	108.53	19.76	184.27	-280.05	-4.01	172.53	24.92	3.40	19.18 ± 0.37 [25]
^{42}Ca	120.46	-371.88	-3.52	109.98	19.67	187.10	-280.80	-4.01	175.47	24.85	3.43	19.7 ± 0.1 [19]
^{44}Ca	122.15	-375.88	-3.54	109.94	19.45	189.81	-281.43	-4.02	177.14	24.69	3.47	19.49 ± 0.34 [18]
^{46}Ca	123.58	-377.80	-3.55	108.54	19.12	190.49	-279.04	-4.01	176.02	24.35	3.51	—
^{48}Ca	125.90	-383.17	-3.57	107.08	18.81	193.97	-279.73	-4.01	176.99	24.18	3.54	19.88 ± 0.16 [25]
^{54}Fe	130.40	-393.27	-3.61	117.90	19.20	200.53	-280.36	-4.02	186.83	24.17	3.64	19.66 ± 0.37 [56]
^{56}Ni	132.18	-397.24	-3.63	118.91	19.12	202.98	-280.54	-4.03	188.24	24.05	3.67	19.1 ± 0.5 [8]
^{58}Ni	130.44	-393.37	-3.59	117.42	18.78	201.13	-280.61	-4.01	186.78	23.69	3.72	18.43 ± 0.15 [57]
^{60}Ni	129.10	-390.27	-3.57	115.47	18.42	199.63	-280.31	-4.00	185.05	23.32	3.76	17.62 ± 0.15 [57]
^{68}Ni	127.54	-385.47	-3.58	105.43	16.80	196.32	-275.46	-3.95	176.58	21.74	3.94	21.1 ± 1.9 [9, 10]
^{64}Zn	126.45	-383.49	-3.54	112.50	17.75	195.54	-277.91	-3.96	180.52	22.48	3.85	18.88 ± 0.79 [56]
^{68}Zn	126.23	-382.87	-3.55	109.41	17.13	195.23	-276.44	-3.95	178.61	21.88	3.93	16.6 ± 0.17 [56]
^{90}Zr	131.04	-387.67	-3.64	111.82	15.99	196.71	-260.62	-3.83	178.32	20.19	4.26	16.9 ± 0.1 [19]
^{92}Zr	130.00	-386.61	-3.62	109.49	15.69	196.75	-263.71	-3.84	177.47	19.97	4.30	16.5 ± 0.1 [19]
^{92}Mo	131.60	-389.18	-3.64	113.18	15.99	197.88	-260.94	-3.82	179.66	20.15	4.29	16.6 ± 0.1 [19]
^{94}Mo	130.44	-386.94	-3.62	111.11	15.71	196.79	-262.17	-3.83	178.02	19.89	4.32	16.4 ± 0.2 [19]
^{96}Mo	129.44	-384.84	-3.61	108.95	15.44	195.70	-262.90	-3.83	176.23	19.63	4.36	16.3 ± 0.2 [19]
^{106}Cd	130.94	-386.97	-3.63	110.82	15.12	196.84	-259.46	-3.80	177.07	19.11	4.48	16.27 ± 0.09 [16]
^{110}Cd	130.31	-385.31	-3.63	108.20	14.74	195.84	-258.52	-3.79	175.09	18.75	4.55	15.94 ± 0.07 [16]
^{112}Cd	130.20	-385.32	-3.63	106.83	14.55	196.02	-258.86	-3.79	174.57	18.60	4.58	15.80 ± 0.05 [16]
^{114}Cd	129.96	-384.33	-3.63	105.24	14.35	195.24	-257.80	-3.78	173.06	18.40	4.61	15.61 ± 0.08 [16]
^{116}Cd	129.78	-383.52	-3.63	103.59	14.15	194.60	-256.86	-3.77	171.60	18.21	4.63	15.44 ± 0.06 [16]
^{100}Sn	134.59	-394.20	-3.69	114.73	15.72	200.14	-256.55	-3.81	179.65	19.67	4.39	—
^{112}Sn	131.64	-388.16	-3.65	110.29	14.82	197.56	-257.83	-3.79	177.06	18.78	4.56	16.2 ± 0.1 [58]
^{114}Sn	131.39	-387.09	-3.65	109.05	14.65	196.74	-256.66	-3.78	175.78	18.60	4.59	16.1 ± 0.1 [58]
^{116}Sn	131.20	-386.23	-3.65	107.73	14.47	196.06	-255.66	-3.77	174.54	18.42	4.62	15.8 ± 0.1 [58]
^{118}Sn	131.22	-386.61	-3.65	106.47	14.30	196.51	-256.22	-3.77	174.26	18.30	4.65	15.8 ± 0.1 [58]
^{120}Sn	131.16	-386.10	-3.65	105.03	14.13	196.07	-255.41	-3.76	173.07	18.13	4.67	15.7 ± 0.1 [58]
^{122}Sn	131.38	-386.80	-3.65	103.71	13.96	196.68	-255.76	-3.77	172.81	18.02	4.70	15.4 ± 0.1 [58]
^{124}Sn	131.54	-386.61	-3.65	102.28	13.80	196.36	-254.40	-3.76	171.64	17.87	4.72	15.3 ± 0.1 [58]
^{132}Sn	133.59	-389.61	-3.69	96.99	13.19	197.57	-249.47	-3.73	169.05	17.42	4.81	—
^{204}Pb	132.82	-384.32	-3.70	97.31	11.50	195.57	-239.26	-3.59	166.26	15.03	5.53	13.98 [59]
^{206}Pb	133.01	-385.04	-3.70	96.55	11.42	196.16	-240.01	-3.60	166.31	14.99	5.54	13.94 [59]
^{208}Pb	133.08	-385.18	-3.70	95.67	11.34	196.23	-240.22	-3.60	165.85	14.93	5.56	13.96 ± 0.2 [60]

we analyze the Sn isotopic chain ($A = 112-124$). Usually the neutron skin thickness in heavy nuclei is defined as

$$\Delta r_{np} = \langle r_n^2 \rangle^{1/2} - \langle r_p^2 \rangle^{1/2}. \quad (33)$$

The "semi-empirical" procedure aims to determine the mean square mass radius $\langle r^2 \rangle$ entering Eq. (2) starting from the experimental values of Δr_{np} . They are measured in different methods [62–67] and shown in Fig. 4 of Ref. [54]. As known, a measurement of the neutron density distributions to a precision and detail comparable to that of the proton one is hardly possible. Having the proton rms radii calculated from the charge radii determined with a high accuracy [61, 68], the neutron rms radii can be obtained from Eq. (33). Then, the matter mean square radius $\langle r^2 \rangle$ are calculated using Eq. (32). The values of the rms radius $\langle r^2 \rangle^{1/2}$ deduced from the procedure are listed in Table III. It is seen that the val-

ues of $\langle r^2 \rangle^{1/2}$ are very close to those for the same Sn isotopes obtained within the HF+BCS calculations with SLy4 interaction and given in Table II. The resulting centroid energies E_{ISGMR} calculated using Eq. (2) are displayed in Fig. 1. In the same figure a comparison with the available experimental data [58] is made. Both Brueckner and BCPM(v) functionals provide excitation energies whose values almost coincide with the calculated ones given in Table II. The small differences in the excitation energy values represent a clear indication of the minimal role of the radius calculated from the empirical data for the neutron skins in Sn isotopes. However, we would like to note the importance of such kind of "alternative" estimations (where possible) avoiding the ambiguities in determination of the neutron rms radii both experimentally and theoretically.

As additional examples of this procedure, we consider

TABLE III: The values of the rms radius $\langle r^2 \rangle^{1/2}$ [Eq. (32)] of Sn isotopes ($A = 112 - 124$) calculated in the procedure based on measurements of the neutron skin thickness Δr_{np} [Eq. (33)] of the same nuclei.

Exp. method	Nuclei	$\langle r^2 \rangle^{1/2}$ [fm]
(p,p) reaction [62, 63]	^{116}Sn	4.624 ± 0.029
	^{124}Sn	4.741 ± 0.030
antiproton atoms [64]	^{112}Sn	4.554 ± 0.011
	^{116}Sn	4.607 ± 0.012
	^{120}Sn	4.635 ± 0.012
	^{124}Sn	4.704 ± 0.012
giant dipole resonance [65]	^{116}Sn	4.549 ± 0.068
	^{124}Sn	4.716 ± 0.067
spin dipole resonance (I) [66, 67]	^{114}Sn	4.544 ± 0.028
	^{116}Sn	4.607 ± 0.035
	^{118}Sn	4.628 ± 0.035
	^{120}Sn	4.671 ± 0.041
	^{122}Sn	4.709 ± 0.042
	^{124}Sn	4.704 ± 0.042
spin dipole resonance (II) [66, 67]	^{114}Sn	4.594 ± 0.006
	^{116}Sn	4.624 ± 0.006
	^{118}Sn	4.658 ± 0.005
	^{120}Sn	4.689 ± 0.006
	^{122}Sn	4.780 ± 0.006
	^{124}Sn	4.686 ± 0.006

two more nuclei, ^{208}Pb and ^{48}Ca , for which the neutron skin thickness has been recently extracted from parity-violating experiments PREX-II [69] and CREX [70], correspondingly. The relatively large neutron skin thickness $\Delta r_{np}(^{208}\text{Pb})=0.283 \pm 0.071$ fm extracted from PREX-II and the small value $\Delta r_{np}(^{48}\text{Ca})=0.121 \pm 0.026 \pm 0.024$ fm extracted from CREX are discussed in Ref. [71]. In this sense, we want to see the influence of the differences between PREX-II and CREX on the monopole excitations in ^{208}Pb and ^{48}Ca nuclei. The values of the rms radii deduced from the procedure are $\langle r^2 \rangle^{1/2}(^{48}\text{Ca})=3.432$ fm and $\langle r^2 \rangle^{1/2}(^{208}\text{Pb})=5.608$ fm, respectively, which are close to the calculated values listed in Table II. For ^{48}Ca nucleus this leads to centroid energies E_{ISGMR} of 19.42 ± 0.170 MeV and 24.97 ± 0.170 MeV when applying Brueckner and BCPM(v) EDF's, while for ^{208}Pb the corresponding values are 11.24 ± 0.088 MeV and 14.80 ± 0.116 MeV. It can be seen that, taking into account the estimated error in the case of Brueckner EDF, the extracted value of the E_{ISGMR} for ^{48}Ca , using the neutron skin thickness reported by the CREX collaboration, fits well with the experimental data.

At this point we turn to the general question, namely, which one, Eq. (1) or Eq. (2) to be used in the calculations of E_{ISGMR} . The point is that there are two different quantities related to the size of the nucleus in Eq. (1) and Eq. (2), namely, $r_0 A^{1/3}$ in Eq. (1) and the root-mean-square (rms) radius $\langle r^2 \rangle^{1/2}$ in Eq. (2). For this purpose we give in what follows the results for E_{ISGMR} obtained from calculations using Eq. (1), where the nu-

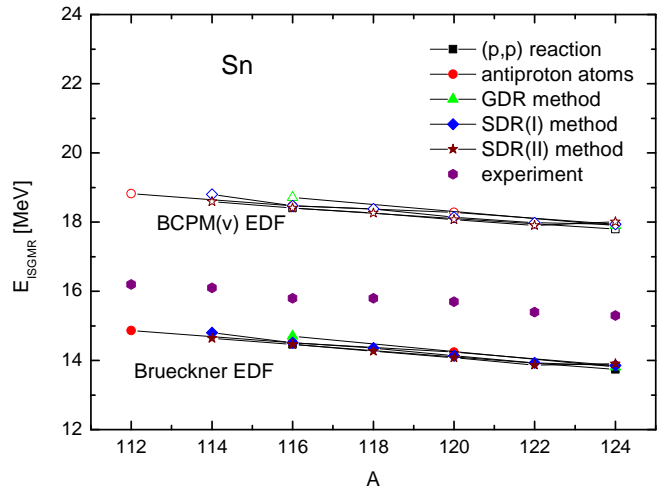


FIG. 1: The centroid energies E_{ISGMR} as a function of the mass number A of Sn isotopes ($A = 112 - 124$) obtained with Brueckner (full symbols) and BCPM(v) (open symbols) EDFs by using the information for the neutron skin thickness extracted from various experiments including (p,p) scattering (squares), antiprotonic atoms (circle), the giant dipole resonance (GDR) method (triangles), and the spin-dipole resonance (SDR) method (diamonds and stars). The experimental data (hexagons) are taken from Ref. [58].

clear radius is given by $R = r_0 A^{1/3}$, r_0 being a radial parameter of density distributions obtained from different experiments. Using the comparison of E_{ISGMR} with the experimental data, we performed a more detailed semi-empirical analysis of the parameter r_0 . We parameterized it in a form:

$$r_0 = (1 + x/A^y) \quad (34)$$

and obtained values of x and y from the fit of E_{ISGMR} with the data for two nuclei in both limits of the considered nuclear range, namely for ^{40}Ca and ^{208}Pb . In the case of ^{40}Ca $r_0=1.205$ fm and in ^{208}Pb $r_0=1.068$ fm. These two conditions lead to the approximated values of $x=2.40$ fm and $y=2/3$. Thus, we obtained the following expression for the radius in the denominator of Eq. (1):

$$R = r_0 A^{1/3} = [1 + 2.40/A^{2/3}] A^{1/3}. \quad (35)$$

This equation can be used for the same range of nuclei. In our opinion, the second term in the right-hand side of Eq. (35) $2.40/A^{1/3}$ is related to the diffuse nuclear surface which changes its range from medium to heavy nuclei. Let us remind at this point the behavior of the nuclear energy per particle B/A ($B/A = a_1 + a_2/A^{1/3} + \dots$, with the known parameters a_1 and a_2) with its volume and surface terms in the right-hand side of this expression. Here we would like to note that our expressions (34) and (35) are for the parameter r_0 , while in Ref. [72] is given an expansion for the charge rms radius.

The dependence of the radial parameter $r_0 = 1 + 2.40/A^{2/3}$ on the mass number between ^{40}Ca and ^{208}Pb

is shown in Fig. 2. The results of the calculations of E_{ISGMR} using Eqs. (1), (34) and (35) in both cases [with the EDFs of Brueckner and BCPM(v)] are listed in Table IV. It can be seen that in this case the results of E_{ISGMR} where the BCPM(v) method is used are in good agreement with the experimental data for almost all of the considered nuclei, which is not the case when the Brueckner EDF is used.

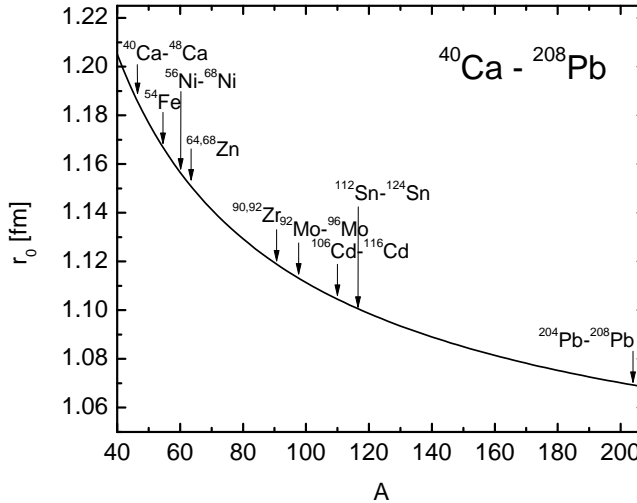


FIG. 2: The dependence of the radius parameter r_0 (in fm) entering Eq. (1) on the mass number A for the considered nuclei between ^{40}Ca and ^{208}Pb .

Here we turn again to the open problem, namely which one of the two procedures based on the use of Eq. (1) or Eq. (2) has to be applied in the theoretical calculations. In our opinion, the definitions in Eq. (1) and Eq. (2) reflect the existing difference between the two usually used meanings of the so-called quantity "radius" of the nucleus. One of them is the rms radius [whose definition is well known, see, e.g., Eq. (31)] and another one is taken usually to be the so-called "half-radius" as $R_{1/2} = r_0 A^{1/3}$, defined by $\rho(R_{1/2}) = \rho(r = 0)/2$. In the present work we make a methodical semi-empirical analysis of the problem. We use in both cases [Eqs. (1) and (2)] the HF+BCS density $\rho(r)$ and the corresponding weight function $|F(x)|^2$ in order to calculate the nuclear incompressibility K^A for a given EDF. In this way, in the case of Eq. (2) the analysis is self-consistent, namely because both quantities K^A and the rms radius are calculated by the HF+BCS nuclear density. In the case of Eq. (1) we use again the same HF+BCS density and K^A . However, we note that in the majority of nuclei it is impossible to measure the central nuclear density $\rho(r = 0)$ and, consequently, to obtain the half-radius $R_{1/2}$ that takes part in Eq. (1). Due to this difficulty we introduced our semi-empirical approach given above and obtained the parameterized form of r_0 [Eq. (34)] and $R_{1/2} = r_0 A^{1/3}$ [Eq. (35)] (including the "surface" term). The existing difference between the rms radius and the $R_{1/2}$ leads to the difference between the energies E_{ISGMR} calculated

TABLE IV: The values of E_{ISGMR} calculated using Brueckner and BCPM(v) density functionals and Eqs. (1), (34) and (35) and compared with the experimental data (the corresponding references are given in Table II).

Nuclei	r_0 [fm]	$r_0 A^{1/3}$ [fm]	$E_{ISGMR}^{\text{Brueckner}}$ [MeV]	$E_{ISGMR}^{\text{BCPM}(v)}$ [MeV]	Exp. [MeV]
^{40}Ca	1.205	4.12	16.29	20.54	19.18 ± 0.37
^{42}Ca	1.199	4.17	16.20	20.46	19.7 ± 0.1
^{44}Ca	1.193	4.21	16.04	20.37	19.49 ± 0.34
^{46}Ca	1.187	4.25	15.79	20.11	—
^{48}Ca	1.182	4.30	15.50	19.93	19.88 ± 0.16
^{54}Fe	1.168	4.41	15.86	19.97	19.66 ± 0.37
^{56}Ni	1.164	4.45	15.79	19.86	19.1 ± 0.5
^{58}Ni	1.160	4.49	15.55	19.61	18.43 ± 0.15
^{60}Ni	1.157	4.53	15.28	19.35	17.62 ± 0.15
^{68}Ni	1.144	4.67	14.16	18.33	21.1 ± 1.9
^{64}Zn	1.150	4.60	14.85	18.82	18.88 ± 0.79
^{68}Zn	1.144	4.67	14.43	18.44	16.6 ± 0.17
^{90}Zr	1.120	5.02	13.57	17.14	16.9 ± 0.1
^{92}Zr	1.118	5.05	13.35	16.99	16.5 ± 0.1
^{92}Mo	1.118	5.05	13.57	17.10	16.6 ± 0.1
^{94}Mo	1.116	5.07	13.39	16.95	16.4 ± 0.2
^{96}Mo	1.114	5.10	13.18	16.77	16.3 ± 0.2
^{106}Cd	1.107	5.24	12.94	16.36	16.27 ± 0.09
^{110}Cd	1.105	5.29	12.67	16.11	15.94 ± 0.07
^{112}Cd	1.103	5.32	12.52	16.00	15.80 ± 0.05
^{114}Cd	1.102	5.34	12.38	15.87	15.61 ± 0.08
^{116}Cd	1.101	5.37	12.21	15.71	15.44 ± 0.06
^{100}Sn	1.111	5.16	13.37	16.73	—
^{112}Sn	1.103	5.32	12.72	16.11	16.2 ± 0.1
^{114}Sn	1.102	5.34	12.60	15.99	16.1 ± 0.1
^{116}Sn	1.101	5.37	12.45	15.85	15.8 ± 0.1
^{118}Sn	1.100	5.40	12.31	15.75	15.8 ± 0.1
^{120}Sn	1.099	5.42	12.18	15.64	15.7 ± 0.1
^{122}Sn	1.098	5.45	12.04	15.54	15.4 ± 0.1
^{124}Sn	1.097	5.47	11.91	15.43	15.3 ± 0.1
^{132}Sn	1.093	5.57	11.39	15.04	—
^{204}Pb	1.069	6.29	10.10	13.21	13.98
^{206}Pb	1.069	6.31	10.03	13.17	13.94
^{208}Pb	1.068	6.33	9.95	13.11	13.96 ± 0.2

by using Eq. (1) or Eq. (2). In this way, following our method to obtain these energies, we think that it is possible to shed more light, at least approximately, on the existing problem. Having in mind the lack of precise data for the neutron (and matter) rms radii for the majority of the considered nuclei and the comparison of the results shown in Table II and Table IV, in our opinion, the use of Eq. (1) with r_0 obtained by a procedure given above [Eqs. (34) and (35), see also Fig. 2] is more preferable.

We should emphasize also that the comparison of the results for E_{ISGMR} obtained using Eq. (1) and both methods for EDF [the Brueckner and BCPM(v) ones] with the data given in Table IV shows the advantage of the BCPM(v) method.

IV. SUMMARY AND CONCLUSIONS

In summary, we have performed a systematic analysis of the isoscalar giant monopole resonance excitation energies in a wide spectrum of nuclei within the microscopic self-consistent Skyrme HF+BCS method with Skyrme SLy4 interaction and pairing correlations, as well as the coherent density fluctuation model. The method of calculations includes three steps. The first one is to determine the incompressibility of infinite nuclear matter [Eq. (16)]. For this purpose, for the potential part of the EDF we use that one of the Brueckner EDF and the one from the EDF of Barcelona-Catania-Paris-Madrid [BCPM(v)]. The second step includes calculations of the necessary incompressibility of finite nuclei within the CDFM scheme averaging the incompressibility of nuclear matter by the weight function $|F(x)|^2$ [Eq. (15)] that is related to the nucleon density distribution [Eq. (10)]. The CDFM provides this possibility being based on the delta-function limit of the generator coordinate method and as extension of the Fermi gas model. In this way, the CDFM allows one to obtain the quantities of finite nuclei (such as the symmetry energy, the incompressibility and others) on the base of the corresponding ones for nuclear matter. As a third step, we perform calculations of the centroid energies of the ISGMR based on the two definitions: the one that uses the radial parameter of the density distributions [Eq. (1)] and the other, in which the excitation energy is expressed through the mean square mass radius of the nucleus in the ground state [Eq. (2)]. The nuclear incompressibility K^A in both cases is calculated by using Eq. (15).

The results for the centroid energy deduced from Eq. (2) in the case of the Brueckner EDF are in good agreement with the data for the lighter isotopes of Ca, Fe, and Ni and acceptable for those of Zn, Mo, and Cd. In the case of BCMP(v) EDF they are comparable for some Pb isotopes and, in particular, for ^{68}Ni nucleus. The excitation energy of ISGMR in ^{68}Ni is located at higher energy (21.1 MeV) for the Ni isotopic chain due to the large fragmentation of the isoscalar monopole strength [9, 10]. Nevertheless, our value of 21.74 MeV reproduces very well the experimental one.

We have analyzed the problems related to the neutron density distributions which cannot be precisely obtained in many cases, as well as the corresponding rms radii. This point is of particular importance for the neutron-rich nuclei, which are the majority of the nuclei considered. Along this line, we performed calculations of the ISGMR energy in cases when data for the neutron skin thickness are available. By using Eq. (2) we found that the results for the Sn isotopic chain ($A = 112 - 124$), as well as for the double-magic ^{48}Ca and ^{208}Pb nuclei recently explored in CREX and PREX experiments, exhibit almost non-sensitivity regarding the extracted mean square mass radius to get values of the centroid energy.

By parametrization of the mass dependence of the radial parameter in the range between ^{40}Ca and ^{208}Pb nu-

clei, we have applied Eq. (1) to calculate the ISGMR energies. A good overall agreement with the experimental data for all considered nuclei is achieved when using the BCMP(v) functional. In conclusion, we would like to note that due to the lack of precise data for the neutron (and matter) rms radii the use of Eq. (1) is more preferable in the theoretical calculations. In addition, we have noted that the comparison of the results for E_{ISGMR} using Eq. (1) and both EDF's of Brueckner and BCMP(v) shows the advantage of the second one. Finally, it is a hope that new data and refined theoretical methods are necessary for the correct description of the breathing modes in medium-heavy nuclei, more specifically the placement of the ISGMR centroid energy.

Acknowledgments

M.K.G. is thankful to Prof. Evgeni Kolomeitsev for the useful discussion. I.C.D wishes to acknowledge partial financial support from the University of Mount Olive Professional Development Fund.

Appendix A

(1) The quantities $S(\rho_0(x))$ [Eq. (13)], $K_{NM}(\rho_0(x))$ [Eq. (17)], $K_{sym}(\rho_0(x))$ [Eq. (20)], $L_{sym}(\rho_0(x))$ [Eq. (21)], $Q(\rho_0(x))$ [Eq. (22)], and $B(\rho_0(x))$ [Eqs. (23) and (24)] obtained in the present work in the case of the Brueckner EDF (Refs. [22, 29, 30, 51], see also e.g. Refs. [37, 42]) are as follows:

$$S(\rho_0(x)) = \frac{5}{9}C\rho_0^{2/3}(x) + b_4\rho_0(x) + b_5\rho_0^{4/3}(x) + b_6\rho_0^{5/3}(x), \quad (\text{A1})$$

$$K_{NM}(\rho_0(x)) = -2C\rho_0^{2/3}(x) + 4b_2\rho_0^{4/3}(x) + 10b_3\rho_0^{5/3}(x), \quad (\text{A2})$$

$$K_{sym}(\rho_0(x)) = -\frac{10}{9}C\rho_0^{2/3}(x) + 4b_5\rho_0^{4/3}(x) + 10b_6\rho_0^{5/3}(x), \quad (\text{A3})$$

$$L_{sym}(\rho_0(x)) = \frac{10}{9}C\rho_0^{2/3}(x) + 3b_4\rho_0(x) + 4b_5\rho_0^{4/3}(x) + 5b_6\rho_0^{5/3}(x), \quad (\text{A4})$$

$$Q(\rho_0(x)) = 8C\rho_0^{2/3}(x) - 8b_2\rho_0^{4/3}(x) - 10b_3\rho_0^{5/3}(x). \quad (\text{A5})$$

The quantity $B(\rho_0(x))$ follows from Eqs. (23) and (24).

In the equations given above:

$$C = \frac{3}{5} \left(\frac{h^2 c^2}{2m} \right) \left(\frac{3\pi^2}{2} \right)^{2/3} \cong 75.05 \text{ [MeV fm}^3\text{]}; \quad (\text{A6})$$

$$\begin{aligned} b_1 &= -741.28, \quad b_2 = 1179.89, \\ b_3 &= -467.54, \quad b_4 = 148.26, \\ b_5 &= 372.84, \quad b_6 = -769.57. \end{aligned} \quad (\text{A7})$$

(2) The quantities of nuclear matter mentioned in the previous point (1) but obtained in the case of the BCPM(v) EDF are as follows:

$$S(\rho_0(x)) = \frac{5}{9} C \rho_0^{2/3}(x) + \left\{ - \sum_{n=1}^5 a_n \left(\frac{\rho_0(x)}{\rho_\infty} \right)^n + \sum_{n=1}^5 b_n \left(\frac{\rho_0(x)}{\rho_{0n}} \right)^n \right\}, \quad (\text{A8})$$

$$K_{NM}(\rho_0(x)) = -2C \rho_0^{2/3}(x) + 9 \sum_{n=1}^5 a_n n(n-1) \left(\frac{\rho_0(x)}{\rho_\infty} \right)^n \quad (\text{A9})$$

$$\begin{aligned} K_{sym}(\rho_0(x)) &= -\frac{10}{9} C \rho_0^{2/3}(x) \\ &+ 9 \left\{ - \sum_{n=1}^5 a_n n(n-1) \left(\frac{\rho_0(x)}{\rho_\infty} \right)^n \right. \\ &\left. + \sum_{n=1}^5 b_n n(n-1) \left(\frac{\rho_0(x)}{\rho_{0n}} \right)^n \right\} \end{aligned} \quad (\text{A10})$$

$$\begin{aligned} L_{sym}(\rho_0(x)) &= \frac{10}{9} C \rho_0^{2/3}(x) - 3 \sum_{n=1}^5 a_n n \left(\frac{\rho_0(x)}{\rho_\infty} \right)^n \\ &+ 3 \sum_{n=1}^5 b_n n \left(\frac{\rho_0(x)}{\rho_{0n}} \right)^n, \end{aligned} \quad (\text{A11})$$

$$\begin{aligned} Q(\rho_0(x)) &= 8C \rho_0^{2/3}(x) \\ &+ 27 \sum_{n=1}^5 a_n n(n-1)(n-2) \left(\frac{\rho_0(x)}{\rho_\infty} \right)^n. \end{aligned} \quad (\text{A12})$$

The quantity $B(\rho_0(x))$ follows from Eqs. (23) and (24).

[1] G. F. Bertsch and S. Das Gupta, Phys. Rep. **160**, 189 (1988).

[2] H. A. Bethe, G. E. Brown, J. Applegate, and J. M. Lattimer, Nucl. Phys. A **324**, 487 (1979).

[3] M. Oertel, M. Hempel, T. Klähn, and S. Typel, Rev. Mod. Phys. **89**, 015007 (2017).

[4] L. Lindblom, Astrophys. J. **398**, 569 (1992).

[5] U. Garg, Acta Physica Polonica B **42**, 659 (2011).

[6] S. K. Biswal and S. K. Patra, Cent. Eur. J. Phys. **12**, 582 (2014).

[7] C. Monrozeau *et al.*, Phys. Rev. Lett. **100**, 042501 (2008).

[8] S. Bagchi *et al.*, Phys. Lett. B **751**, 371 (2015).

[9] M. Vandebruck *et al.*, Phys. Rev. Lett. **113**, 032504 (2014).

[10] M. Vandebruck *et al.*, Phys. Rev. C **92**, 024316 (2015).

[11] J. Arroyo *et al.*, Phys. Rev. C **111**, 014308 (2025).

[12] O. Bohigas, A. Lane, and J. Martorell, Phys. Rep. **51**, 267 (1979).

[13] J. P. Blaizot, Phys. Rep. **64**, 171 (1980).

[14] U. Garg and G. Colò, Prog. Part. Nucl. Phys. **101**, 55 (2018).

[15] T. Li *et al.*, Phys. Rev. C **81**, 034309 (2010).

[16] D. Patel, U. Garg, M. Fujiwara, H. Akimune, G. P. A. Berg, M. N. Harakeh, M. Itoh, T. Kawabata, K. Kawase, B. K. Nayak, T. Ohta, H. Ouchi, J. Piekarewicz, M. Uchida, H. P. Yoshida, M. Yosoi, Phys. Lett. B **718**, 447 (2012).

[17] J. P. Blaizot, D. Gogny, and B. Grammaticos, Nucl. Phys. A **265**, 315 (1976).

[18] J. Button, Y.-W. Lui, D. H. Youngblood, X. Chen, G. Bonasera, and S. Shlomo, Phys. Rev. C **96**, 054330 (2017).

[19] K. B. Howard, U. Garg, Y. K. Gupta, and M. N. Harakeh, Eur. Phys. J. A **55**, 228 (2019).

[20] K. B. Howard *et al.*, Phys. Lett. B **801**, 135185 (2020).

[21] K. B. Howard *et al.*, Phys. Lett. B **807**, 135608 (2020).

[22] K. A. Brueckner, M. J. Giannoni, and R. J. Lombard, Phys. Lett. **31B**, 97 (1970).

[23] S. Shlomo, Pramana-J. Phys. **57**, 557 (2001).

[24] Lie-Wen Chen and Jian-Zhong Gu, J. Phys. G **39**, 035104 (2012).

[25] M. R. Anders and S. Shlomo, J. Phys.: Conf. Ser. **420**, 012051 (2013).

[26] Jun Su, Long Zhu, and Chenchen Guo, Phys. Rev. C **98**, 024315 (2018).

[27] G. Colò, D. Gambacurta, W. Kleinig, J. Kvasil, V. O. Nesterenko, and A. Pastore, Phys. Lett. B **811**, 135940 (2020).

[28] G. Bonasera, S. Shlomo, D. H. Youngblood, Y.-W. Lui, J. Button, and X. Chen, Nucl. Phys. A **1010**, 122159 (2021).

[29] K. A. Brueckner, J. R. Buchler, S. Jorna, and R. J. Lombard, Phys. Rev. **171**, 1188 (1968).

[30] K. A. Brueckner, J. R. Buchler, R. C. Clark, and R. J. Lombard, Phys. Rev. **181**, 1543 (1969).

[31] M. Baldo, L. M. Robledo, and X. Viñas, Eur. Phys. J. A **59**, 156 (2023).

[32] M. Baldo, L. M. Robledo, P. Schuck, and X. Viñas, Phys. Rev. C **87**, 064305 (2013).

[33] M. Baldo, L. M. Robledo, P. Schuck, and X. Viñas, Phys. Rev. C **95**, 014318 (2017).

[34] A. N. Antonov, V. A. Nikolaev, and I. Zh. Petkov, Bulg.

J. Phys. **6**, 151 (1979); Z. Phys. A **297**, 257 (1980); *ibid* **304**, 239 (1982); Nuovo Cimento A **86**, 23 (1985); Bulg. J. Phys. **18**, 107 (1991); A. N. Antonov *et al.*, *ibid* **102**, 1701 (1989); A. N. Antonov, D. N. Kadrev, and P. E. Hodgson, Phys. Rev. C **50**, 164 (1994).

[35] A. N. Antonov, P. E. Hodgson, and I. Zh. Petkov, *Nucleon Momentum and Density Distributions in Nuclei* (Clarendon Press, Oxford, 1988); *Nucleon Correlations in Nuclei* (Springer-Verlag, Berlin-Heidelberg-New York, 1993).

[36] J. J. Griffin and J. A. Wheeler, Phys. Rev. **108**, 311 (1957).

[37] M. K. Gaidarov, A. N. Antonov, P. Sarriguren, and E. Moya de Guerra, Phys. Rev. C **84**, 034316 (2011).

[38] M. K. Gaidarov, A. N. Antonov, P. Sarriguren, and E. Moya de Guerra, Phys. Rev. C **85**, 064319 (2012).

[39] M. K. Gaidarov, P. Sarriguren, A. N. Antonov, and E. Moya de Guerra, Phys. Rev. C **89**, 064301 (2014).

[40] A. N. Antonov, M. K. Gaidarov, P. Sarriguren, and E. Moya de Guerra, Phys. Rev. C **94**, 014319 (2016).

[41] A. N. Antonov, D. N. Kadrev, M. K. Gaidarov, P. Sarriguren, and E. Moya de Guerra, Phys. Rev. C **98**, 054315 (2018).

[42] I. C. Danchev, A. N. Antonov, D. N. Kadrev, M. K. Gaidarov, P. Sarriguren, and E. Moya de Guerra, Phys. Rev. C **101**, 064315 (2020).

[43] M. K. Gaidarov, I. Moumene, A. N. Antonov, D. N. Kadrev, P. Sarriguren, and E. Moya de Guerra, Nucl. Phys. A **1004**, 122061 (2020).

[44] M. K. Gaidarov, A. N. Antonov, D. N. Kadrev, P. Sarriguren, and E. Moya de Guerra, Chapter in *Nuclear Structure Physics*, ed. by A. Shukla and S. K. Patra, (CRC Press, Taylor & Francis Group, 2020), pp.93–120 (2020).

[45] M. K. Gaidarov, E. Moya de Guerra, A. N. Antonov, I. C. Danchev, P. Sarriguren, and D. N. Kadrev, Phys. Rev. C **104**, 044312 (2021).

[46] M. K. Gaidarov, M. V. Ivanov, Y. I. Katsarov, and A. N. Antonov, Astronomy **2**, 1 (2023).

[47] S. Stringari, Phys. Lett. B **108**, 232 (1982).

[48] A. E. L. Dieperink, Y. Dewulf, D. Van Neck, M. Waroquier, and V. Rodin, Phys. Rev. C **68**, 064307 (2003).

[49] Lie-Wen Chen, Phys. Rev. C **83**, 044308 (2011).

[50] G. Colò, U. Garg, H. Sagawa, Eur. Phys. J. A **50**, 26 (2014).

[51] K. A. Brueckner, S. A. Coon, and J. Dabrowski, Phys. Rev. **168**, 1184 (1968).

[52] E. Chabanat, P. Bonche, P. Haensel, J. Meyer, and R. Schaeffer, Nucl. Phys. A **635**, 231 (1998).

[53] D. Vautherin, Phys. Rev. C **7**, 296 (1973).

[54] P. Sarriguren, M. K. Gaidarov, E. Moya de Guerra, and A. N. Antonov, Phys. Rev. C **76**, 044322 (2007).

[55] F. Sammarruca and R. Millerson, Universe **8**, 133 (2022).

[56] J. Button *et al.*, Phys. Rev. C **100**, 064318 (2019).

[57] Y.-W. Lui *et al.*, Phys. Rev. C **73**, 014314 (2006).

[58] Li-Gang Cao, H. Sagawa, and G. Colò, Phys. Rev. C **86**, 054313 (2012).

[59] M. Fujiwara *et al.*, AIP Conf. Proc. **1377**, 164 (2011).

[60] D. H. Youngblood, Y.-W. Lui, H. L. Clark, B. John, Y. Tokimoto, and X. Chen, Phys. Rev. C **69**, 034315 (2004).

[61] H. De Vries, C. W. De Jager, and C. De Vries, At. Data Nucl. Data Tables **36**, 495 (1987).

[62] L. Ray, Phys. Rev. C **19**, 1855 (1979).

[63] G. W. Hoffmann *et al.*, Phys. Rev. Lett. **47**, 1436 (1981).

[64] A. Trzcinska, J. Jastrzebski, P. Lubinski, F. J. Hartmann, R. Schmidt, T. von Egidy, and B. Klos, Phys. Rev. Lett. **87**, 082501 (2001).

[65] A. Krasznahorkay *et al.*, Nucl. Phys. A **567**, 521 (1994).

[66] A. Krasznahorkay *et al.*, Phys. Rev. Lett. **82**, 3216 (1999).

[67] A. Krasznahorkay *et al.*, Nucl. Phys. A **731**, 224 (2004).

[68] J. D. Patterson and R. J. Peterson, Nucl. Phys. A **717**, 235 (2003).

[69] D. Adhikari *et al.*, Phys. Rev. Lett. **126**, 172502 (2021).

[70] The CREX Collaboration, Phys. Rev. Lett. **129**, 042501 (2022).

[71] R. Machleidt and F. Sammarruca, Progr. Part. Nucl. Phys. **137**, 104117 (2024).

[72] I. Angeli and K.P. Marinova, At. Data Nucl. Data Tables **99**, 69 (2013).